

## Catfish: A Monte Carlo simulator for black holes at the LHC

M. Cavaglià<sup>a</sup>, R. Godang<sup>a,b</sup>, L. Cremaldi<sup>a</sup> and D. Summers<sup>a</sup>

<sup>(a)</sup> *Department of Physics and Astronomy, University of Mississippi  
University, MS 38677-1848, USA*

<sup>(b)</sup> *University of South Alabama, Department of Physics, Mobile AL 36688, USA*

### Abstract

We present a new Fortran Monte Carlo generator to simulate black hole events at CERN's Large Hadron Collider. The generator interfaces to the PYTHIA Monte Carlo fragmentation code. The physics of the BH generator includes, but not limited to, inelasticity effects, exact field emissivities, corrections to semiclassical black hole evaporation and gravitational energy loss at formation. These features are essential to realistically reconstruct the detector response and test different models of black hole formation and decay at the LHC.

PACS: 04.80.Cc, 04.50.+h, 12.60.-i, 13.85.-t

Keywords: Extra dimensions, black holes, hadron colliders, Monte Carlo methods

# 1 Introduction

The fundamental scale of gravity may be much lower than the measured gravitational scale [1]. In scenarios with large or warped extra dimensions, the observed weakness of gravity is explained by assuming that Standard Model (SM) fields are constrained to propagate on a four-dimensional submanifold, whereas gravitons propagate in the higher-dimensional spacetime [2]. If the gravitational coupling constant is of the order of few TeVs, super-Planckian events at CERN's LHC could lead to the formation of subnuclear Black Holes (BHs) [3] and branes [4] (For reviews and further references, see Refs. [5, 6]).

The semiclassical limit of super-Planckian scattering suggests that the cross section for creation of a BH or brane with radius  $R$  is approximately equal to the geometrical Black Disk (BD) cross section  $\sigma_{BD}(s, n) = \pi R^2(s, n)$ , where  $\sqrt{s}$  is the Center of Mass (CM) energy of the colliding quanta and  $n$  is the number of extra dimensions. The semiclassical Hawking effect [7] provides a thermal decay mechanism for BHs, thus allowing their detection. The spectrum of massive excitations in string theories suggests that branes may also decay thermally [8]. Under the most favorable circumstances, the BH event rate at the LHC should be comparable to the  $t\bar{t}$  event rate.

Until now, numerical studies of observational signatures have used Monte Carlo (MC) generators implementing the semiclassical picture outlined above. Currently, there are two MC generators for BH production at particle colliders: TRUENOIR [9] and CHARYBDIS [10]. However, recent results have modified significantly our understanding of BH formation and evolution. It is thus timely and worthwhile to examine the observational signatures of BH events beyond the simple semiclassical picture. To this purpose, we have developed a new Fortran MC generator for BH events at the LHC which includes many of the accepted theoretical results in the literature. The generator, called CATFISH (Collider grAviTational FIeld Simulator for black Holes), interfaces to the PYTHIA MC fragmentation code [11] using the Les Houches interface [12]. CATFISH allows the most accurate description of BH events at the TeV scale up-to-date. Its flexibility permits to compare the signatures of different theoretical models of BH production. MC generators with similar characteristics of CATFISH have already been successfully utilized to simulate BH production in ultrahigh-energy cosmic ray air showers [13] and in lepton colliders [14]. Precompiled executable versions of CATFISH (Linux and Mac OS platforms) are available at the CATFISH website <http://www.phy.olemiss.edu/GR/catfish>.

## 2 Basics of BH formation and evolution

In this section we follow Ref. [13] and briefly review the basics of BH formation and evolution.

### 2.1 BH formation and cross section at parton level

Thorne's hoop conjecture [15] states that an event horizon forms when a mass  $M$  is compacted into a region with circumference smaller than twice the Schwarzschild radius  $R(M)$  in any direction. At the LHC, this process can be achieved by scattering two partons  $ij$  with CM energy larger than  $M$  and impact parameter smaller  $b$  than  $R$ . The BH event is described by the inelastic process  $ij \rightarrow \text{BH} + E(X)$ , where  $E(X)$  denotes the collisional energy that does not fall beyond the event horizon. Due to the gravitational nature of the process, this energy includes mainly a bulk component of gravitational radiation, although non-SM gauge fields and a brane component of SM fields cannot be excluded. If  $E(X)$  is zero, the hoop conjecture implies that the parton cross section

for BH production is equal to the geometrical BD cross section,  $\sigma_{ij}(s, n) = \sigma_{BD}(s_{ij}, n)\theta(R(s_{ij}) - b)$ . If  $E(X) \neq 0$ , the cross section is generally smaller and depends on the impact parameter. Note that this treatment is valid only if the BH is larger than the Compton length of the colliding quanta. (For discussions on the effect of wave packet size on the BH formation process, see Refs. [16].) A precise calculation of the collisional energy loss is essential to understanding BH formation.

The hoop conjecture has been tested by different methods [6], the most popular one being the Trapped-Surface (TS) approach [17, 18, 19], The TS model gives a bound on the inelasticity by modeling the incoming partons as two Aichelburg-Sexl shock waves [20]. The Aichelburg-Sexl wave is obtained by boosting the Schwarzschild solution to the speed of light at fixed energy. The resulting metric describes a plane-fronted gravitational shock wave corresponding to the Lorentz-contracted longitudinal gravitational field. The parton scattering is simulated by superposing two shock waves traveling in opposite directions. The union of these shock waves defines a closed TS that allows to set a lower bound on the initial BH mass  $M_{BH}$ . The collisional energy loss depends on the impact parameter and increases as the number of spacetime dimensions increases. The BH mass monotonically decreases with the impact parameter from a maximum of about 60-70% of the CM energy for head-on collisions.

The TS result is consistent within one order of magnitude with the hoop conjecture. However, this approach neglects mass, spin, charge and finite-size effects of the incoming partons. Size and spin effects are expected to be mostly relevant around the Planck energy. Charge effects could dominate at higher energy. The pointlike approximation fails for directions transversal to the motion [21]. Even with these assumptions, the TS model provides only a lower bound on  $M_{BH}$ . Independent estimates of the gravitational collisional energy loss are possible through alternative approaches. The gravitational energy emission in a hard instantaneous collision can be evaluated in the linearized limit [22]. This computation suggests that the TS method overestimates the gravitational energy emitted in the process. For head-on collisions, the instantaneous method predicts that the gravitational energy loss is only about 10% of the CM energy. This result is in agreement with perturbative calculations modeling the parton-parton collision as a plunge of a relativistic test particle into a BH with mass equal to the CM energy [23].

In conclusion, a conservative estimate of gravitational loss in relativistic scattering at parton level gives a BH mass ranging between 60% and 100% of the CM energy. The TS result and the BD result can be considered as the lower and upper bounds on  $M_{BH}$ , respectively.

## 2.2 Cross section at nucleon level

The total cross section for a super-Planckian BH event involving two nucleons is obtained by integrating the parton cross section over the Parton Distribution Functions (PDFs). If the BH mass depends on the impact parameter, the generally accepted formula for the total cross section of the pp process is

$$\sigma_{pp \rightarrow BH}(s, n) = \sum_{ij} \int_0^1 2z dz \int_{x_m}^1 dx \int_x^1 \frac{dx'}{x'} f_i(x', Q) f_j(x/x', Q) F \sigma_{BD}(xs, n), \quad (1)$$

where  $f_i(\cdot, Q)$  are the PDFs with four-momentum transfer squared  $Q$  [24, 25] and  $z$  is the impact parameter normalized to its maximum value. The cutoff at small  $x$  is  $x_m = M_{min}^2/(sy^2(z))$ , where  $y(z)$  and  $M_{min}$  are the fraction of CM energy trapped into the BH and the minimum-allowed mass of the gravitational object, respectively.  $F$  is a form factor. The total cross section for the BD model is obtained by setting  $F = 1$  and  $y^2(z) = 1$ .

Different sets of PDFs are defined in the literature. The PDFs are not known at energies above the TeV and for values of momentum transfer expected in BH formation. Equation (1) is usually calculated by imposing a cut-off at these values. The PDFs also suffer from uncertainties at any momentum transfer ( $\sim 10\%$ ) [26] and from the ambiguity in the definition of  $Q$  [27]. The momentum transfer is usually set to be  $M_{BH}$  or the Schwarzschild radius inverse. The uncertainty due to this ambiguity is about  $\sim 10 - 20\%$ .

The form factor and the amount of trapped energy depend in principle on energy, gravitational scale, geometry and physical properties of the spacetime. The TS method gives numerical values of order unity for these quantities. (See Refs. [17, 18] and discussion above). However, these results depend on the way the TS is identified. Other models [28] give values which are more or less consistent with the TS method. It is common practice in the literature to either choose the TS result or the simple BD model.

The lower cutoff on the fraction of the nucleon momentum carried by the partons is set by the minimum-allowed formation mass of the gravitational object,  $M_{min}$ . This threshold is usually considered to be roughly equal to the minimum mass for which the semiclassical description of the BH is valid. However, this argument is based on Hawking's semiclassical theory and may not be valid at energies equal to few times the Planck mass. For example, the existence of a minimum spacetime length  $l_m$  implies the lower bound on the BH mass [29, 30]:

$$M_{ml} = \frac{n+2}{8\Gamma\left(\frac{n+3}{2}\right)} (\sqrt{\pi} l_m M_\star/2)^{n+1} M_\star, \quad (2)$$

where  $M_\star$  is the fundamental Planck mass. BHs with mass less than  $M_{ml}$  do not exist, since their horizon radius would fall below the minimum-allowed length. Note that  $M_{ml}$  grows as a power of  $l_m^{n+1}$  at fixed  $M_\star$ . Therefore,  $M_{min}$  may be much larger than  $M_\star$  for higher-dimensional spacetimes.

### 2.3 BH evolution

It is believed that the decay of microscopic BHs happens in four distinct stages: I. radiation of excess multipole moments (balding phase); II. spin-down; III. Hawking evaporation; IV. final explosion or formation of a BH remnant.

Although some progress has been made, a quantitative description of the balding phase and the spin-down phase is not fully known. For example, the emission of radiation from a  $(n+4)$ -dimensional rotating BH on the brane is not known for spin-2 fields [31]. Due to these limitations, balding phase and spin-down phase effects are not implemented in the current version of CATFISH. It should be stressed, however, that balding and spin-down effects could play an important role in BH phenomenology at the LHC.

Many papers have been devoted to the investigation of BH evaporation in higher dimensions [32], leading to a better understanding of the Hawking phase. Field emissivities for all SM fields have recently been calculated [33]. For non rotating BHs and the minimal  $SU(3) \times SU(2) \times U(1)$  SM, most of the BH mass is radiated as SM quanta on the brane, although the gravitational emission in the bulk cannot be neglected for high  $n$ . Two points should be stressed [34]: (i) it is not clear what is the effect of rotation on BH emissivities; (ii) the field content at trans-Planckian energies is not known. Onset of supersymmetry, for example, could lead to other evaporation channels and large emission of undetectable non-SM quanta during the decay phase even in absence of rotation [35].

Quantum gravitational effects and BH recoil [36] could also affect the emission of visible quanta on the brane. Examples of quantum gravitational effects are quantum thermal fluctuations and

corrections to the Hawking thermodynamics due to the existence of a minimum length [30]. The existence of a minimum scale of the order of the Planck length [37] is a common consequence of most (if not all) theories of quantum gravity such as string theory, non-commutative geometry, canonical quantum gravity, etc. The presence of a cutoff at the Planck scale leads to a modification of the uncertainty principle. Since the Hawking thermodynamical quantities can be derived by applying the uncertainty principle to the BH, the existence of a minimum length leads to corrections in the thermodynamical quantities [29, 30].

At the end of the Hawking phase, the BH is expected to either non-thermally decay in a number  $n_p$  of hard quanta or leave a remnant. In either case, the lack of a theory of quantum gravity does not allow more than a phenomenological treatment. The final decay is usually described by setting a cutoff on the BH mass of the order of the Planck mass,  $Q_{min} \sim M_\star$ , and equally distributing the energy  $Q_{min}$  to  $n_p$  quanta. Since the decay is non-thermal, and in absence of any guidance from a theory of quantum gravity, the quanta are democratically chosen among the SM Degrees of Freedom (DoFs). Note that  $Q_{min}$  does not necessarily coincide with  $M_{min}$ . The former gives the threshold for the onset of quantum gravity effects in the decay phase, whereas the latter gives the minimum-allowed mass of the classical BH in the formation process. From the above definitions, it follows  $M_{min} \geq Q_{min}$ . The existence of a minimum length gives a natural means to set  $Q_{min}$ . In that case, the modified thermodynamical quantities determine the endpoint of Hawking evaporation when the BH mass reaches  $M_{ml}$ . This mass can be identified with the mass of the BH remnant.

### 3 BH generator

In this section we list the main characteristics of the CATFISH generator. The physics of BH formation and decay is determined by the following set of external parameters and switches in the MC code:

- Fundamental Planck scale ( $M_\star$ )
- Number of large extra dimensions ( $n$ )
- Gravitational loss at formation
- Gravitational loss model
- Minimum BH mass at formation ( $M_{min}$ )
- Quantum BH mass threshold at evaporation ( $Q_{min}$ )
- Number of quanta at the end of BH decay ( $n_p$ )
- Momentum transfer model in parton collision
- Conservation of electromagnetic (EM) charge
- Minimum spacetime length ( $\alpha$ )

These parameters are briefly explained below.

#### 3.1 BH formation and parton cross section

The MC generator does not require any lower or upper bound on the Planck mass  $M_\star$ . However, experimental constraints exclude values of  $M_\star \lesssim 1$  TeV [38, 39] and BHs do not form at the LHC if  $M_\star > 14$  TeV. Models with one or two flat large extra dimensions are excluded experimentally [38, 39]. Most of the theoretical models are limited to  $n \leq 7$ . Therefore, the allowed number of extra dimensions  $n$  ranges from 3 to 7. (Warped scenarios such as the Randall-Sundrum models [40] with a single extra dimension are experimentally viable. However, the extra dimension is warped.

Since most of the results in the literature concerning black holes at colliders have been derived for a flat extra-dimensional scenario, we choose not to allow  $n = 1$  to mimic BH production in warped models.)

CATFISH includes three models for BH formation and cross section: BD, Yoshino-Nambu (YN) TS model [17], and Yoshino-Rychkov (YR) improved TS model [18]. The minimum BH mass  $M_{min}$  is set in units of  $M_*$  or, if a minimum length is present,  $M_{ml}$ :  $X_{min} = M_{min} \geq \text{Max}(M_*, M_{ml})$ . This parameter is always larger than one.

### 3.2 Total and differential cross section

The distribution of the initial BH masses is sampled from the differential cross section  $d\sigma/dM_{BH}$ . CATFISH uses the (stable) cteq5 PDF distribution [24, 41]. The use of different PDF distributions should not significantly affect the total and differential cross sections. Therefore, different PDF distributions are not implemented in the code. The uncertainty due to the choice of the momentum transfer is generally larger. A logical switch allows a choice between  $M_{BH}$  or inverse Schwarzschild radius, as the definition of momentum transfer. The part of CM energy of the pp collision which is not trapped or lost in gravitational radiation at formation forms the beam remnant, which is hadronized by PYTHIA.

### 3.3 BH evaporation

Due to the lack of results for the balding and spin-down phases described above, energy losses in these stages are assumed to be either negligible or included in the energy loss during formation. Since the TS model likely overestimates the actual energy loss, this is a reasonable assumption. However, we stressed above that balding and spin-down effects could significantly affect the event signatures. We plan to include balding and spin-down effects in updated versions of the code, as soon as theoretical results become available.

A similar approach is used in the Hawking phase, where the MC uses only the emissivities of non-rotating spherically-symmetric BHs [33]. (Emissivities for rotating BHs are not fully known.) This is a reasonable assumption, given that the BH is expected to be bald and spinless by the time the evaporation phase begins. Moreover, intrinsic uncertainties in event reconstruction should hide at least some of the differences between rotating and non-rotating field emissivities. The particle content at trans-Planckian energy is assumed to be the minimal  $SU(3) \times SU(2) \times U(1)$  SM with three families and a single Higgs boson on a thin brane. For black holes with mass  $\sim$  few TeV the Hawking temperature is generally above 100 GeV. Therefore, all SM DoFs can be considered massless. (Considering massive gauge bosons does not affect the conclusions significantly.) The spin-0, -1/2 and -1 DoFs on the brane are 1 (Higgs field), 90 (quarks + charged leptons + neutrinos) and 27 (gauge bosons), respectively. The longitudinal DoFs of the weak bosons are included in the counting. The DoFs  $c_i$  and the relative emissivities  $\Gamma_{\mathcal{P}_i}$  and  $\Gamma_{\mathcal{R}_i}$  [33] are given in Table I – III, respectively. In the notations of Ref. [33] the total decay multiplicity is [34]

$$N = \frac{(n+1)S}{4\pi} \frac{\sum_i c_i \mathcal{R}_i \Gamma_{\mathcal{R}_i}}{\sum_j c_j \mathcal{P}_j \Gamma_{\mathcal{P}_j}}, \quad (3)$$

where  $S$  is the initial entropy of the BH and the emissivity normalizations for spin- $s$  fields are:

$$\mathcal{P}_s = \begin{cases} 2.9 \times 10^{-4} & s = 0 \\ 1.6 \times 10^{-4} & s = 1/2 \\ 6.7 \times 10^{-5} & s = 1 \\ 1.5 \times 10^{-5} & s = 2 \end{cases}, \quad \mathcal{R}_s = \begin{cases} 1.4 \times 10^{-3} & s = 0 \\ 4.8 \times 10^{-4} & s = 1/2 \\ 1.5 \times 10^{-4} & s = 1 \\ 2.2 \times 10^{-5} & s = 2 \end{cases}. \quad (4)$$

The decay multiplicities per species  $N_i$  are

$$N_i = N \frac{c_i \mathcal{R}_i \Gamma_{\mathcal{R}_i}}{\sum_j c_j \mathcal{R}_j \Gamma_{\mathcal{R}_j}}. \quad (5)$$

The presence of a minimum length affects the evaporation phase. CATFISH uses the dimensionless parameter  $\alpha = l_m M_\star/2$  to determine the minimum length. If there is no minimum length, i.e.  $\alpha = 0$ , the MC evaporates the BH according to the Hawking theory (with varying temperature). Alternatively, the BH evolution proceeds according to the modified thermodynamics of Ref. [29, 30]. In both cases the evaporation ends when the BH reaches the mass  $Q_{min}$ . This is set in units of  $M_\star$  ( $M_{ml}$ ) if the minimum length is zero (nonzero). Note that the BH minimum formation mass  $M_{min}$  and the endpoint of Hawking evaporation  $Q_{min}$  are independent parameters.

Four-momentum is conserved at each step in the evaporation process by taking into account the recoil of the BH on the brane due to the emission of the Hawking quanta. The initial energy of the BH is distributed democratically among all the Hawking quanta with a random smearing of  $\pm 10\%$ . This smearing factor is introduced on a purely phenomenological basis to take into account quantum uncertainties in the emission of each quantum.

### 3.4 BH final decay

The MC code allows for two different choices of final BH decay: Final explosion in a number  $n_p$  of quanta or BH remnant. If  $n_p = 0$ , the BH settles down to a remnant with mass  $Q_{min}$ . If  $n_p = 2 \dots 18$ , the BH decays in a number  $n_p$  of quanta by a  $n$ -body process with total CM energy equal to  $Q_{min}$ .

CATFISH allows conservation of color and EM charges. Color charge is always conserved. A logical switch controls conservation of EM charge in the decay process (Hawking evaporation + final decay). The purpose of this switch is to allow for the existence of a charged or neutral BH remnant.

If the EM charge switch is set to **FALSE**, there is no constraint on the total charge of the emitted quanta  $Q_E$ . If  $n_p = 0$ , physical charge conservation implies the relation  $Q_E + Q_R + Q_B = 2e$ , where  $Q_E$  is the total charge of the Hawking quanta,  $Q_R$  is the charge of the BH remnant and  $Q_B$  is the charge of the beam remnant. In that case, the BH remnant can be either neutral or charged, depending on the event. The choice  $n_p \neq 0$  and no charge conservation (**FALSE**) is unphysical and should be avoided.

If the EM charge switch is set to **TRUE**, the absolute value of the total charge of the emitted quanta is  $|Q_E| \leq 4e/3$ , i.e. the maximum possible total charge of the scattering partons. In that case, the excess charge  $2e - Q_E$  is assigned to the beam remnant and, if  $n_p = 0$ , the BH remnant is considered neutral. This is justified from the fact that local charges should have been shed earlier in the evaporation process. (See, however, Ref. [42] for a different viewpoint.) It should be stressed that the collider phenomenology of a charged remnant is not known and it is not clear how to track it in a detector in a meaningful way.

	$c_i$
Quarks	72
Charged leptons	12
Neutrinos	6
Photon	2
EW bosons	9
Gluons	16
Higgs	1
Graviton	1

Table 1: DoFs  $c_i$  for the SM fields on a thin brane. The graviton is assumed to propagate in all  $(n + 4)$  dimensions. Following Ref. [33], the  $(n + 4)(n + 1)/2$  graviton helicities are included in the emissivities (see Table 2 and 3 below). Therefore, the graviton counts as one DoF. Longitudinal DoFs are included in the EW boson counting.

	n=3	n=4	n=5	n=6	n=7
Higgs	1	1	1	1	1
Fermions	0.89	0.87	0.85	0.84	0.82
Gauge Bosons	1.0	1.04	1.06	1.06	1.07
Gravitons	2.7	4.8	8.8	17.7	34.7

Table 2: Fraction of radiated power per DoF and species  $i$ ,  $\Gamma_{\mathcal{P}_i}$ , normalized to the Higgs field. The graviton values include all the helicity states. (From Ref. [33].)

	n=3	n=4	n=5	n=6	n=7
Higgs	1	1	1	1	1
Fermions	0.78	0.76	0.74	0.73	0.71
Gauge Bosons	0.83	0.91	0.96	0.99	1.01
Graviton	0.91	1.9	2.5	5.1	7.6

Table 3: Fraction of emission rates per DoF and species  $i$ ,  $\Gamma_{\mathcal{R}_i}$ , normalized to the Higgs field. The graviton values include all the helicity states. (From Ref. [33].)

### 3.5 Event simulation

The steps to simulate a BH event are:

1. Two proton beams of energy  $7 + 7$  TeV are injected in the Monte Carlo (CM frame).
2. The cross section for the process is computed.
3. The initial black hole mass is sampled from the differential cross section (see Fig. 1).
4. The black hole is decayed through the Hawking mechanism and final hard event (or black hole remnant).
5. The unstable quanta from the black hole and beam remnant are hadronized or decayed instantaneously by PYTHIA. Initial- and final-state radiation are included in PYTHIA's output.



## 4 Analysis of BH events

Signatures of BH events at the LHC have been investigated in a number of papers [43, 44, 45, 46, 47, 48] using the TRUENOIR [9] or CHARYBDIS [10] generators. In this section we present some results for CATFISH. We focus on a purely statistical analysis of variables which allow an easy comparison with previous results obtained with the CHARYBDIS generator. A more refined analysis of other detector response-dependent signatures such as back-to-back di-jet suppression, di-lepton events ( $\mu^+\mu^-$ ,  $\mu^+e^-$ ,  $\mu^+e^+$ , ...) will be presented in a future publication [49].

### 4.1 Visible energy and visible/missing transverse momentum

Missing transverse momentum ( $\cancel{P}_T$ ) and visible transverse momentum of leptons and hadrons are important signatures of BH production in particle colliders. Figure 2 shows the simulation output for 10,000 events at the LHC with the following parameters (benchmark):

$$n = 6, \quad M_{min} = Q_{min} = M_\star, \quad n_p = 4, \quad \alpha = 0,$$

BD cross section and conservation of EM charge. The momentum transfer is set to be equal to the Schwarzschild radius inverse. Particles in the beam pipe and in the initial-radiation phase has been removed by imposing  $P_T$  cuts of 5 GeV and 15 GeV on leptons ( $e, \mu$ ) and photons + hadrons ( $\gamma, h$ ), respectively. (These choices of cuts and momentum transfer apply to all simulations throughout the paper.) The plots show the total visible energy distribution,  $\cancel{P}_T$  and the visible transverse momentum of leptons ( $e, \mu$ ) and photons + jets ( $\gamma, h$ ) with varying fundamental scale  $M_\star = 1 \dots 3$  TeV.

The plots in Fig. 2 for the BD model can be used to compare CATFISH with previous BH generators. For example, these results are in good agreement with results obtained with CHARYBDIS [44]. BH events may show a large amount of transverse momentum up to several TeV, depending on the value of the fundamental scale and the number of extra dimensions.

In the absence of a BH remnant and for the BD model, the missing transverse momentum is due to undetectable quanta (gravitons + neutrinos) during the evaporation phase. Detectable quanta are originated in the Hawking and final decay phase with an upper bound to their multiplicity given by  $N + n_p$ , where  $N$  is given in Eq. (3). The bulk of BH events is characterized by light, low-entropy BHs. Since the graviton and neutrino channels accounts only for a small fraction of the total multiplicity in the decay phase, only rare high-mass events show a large amount of missing transverse momentum. A rough counting of DoFs shows that the hadronic-to-leptonic decay ratio of a BH event should be approximately 5:1. The prevalence of the hadronic channel on the leptonic channel is evident from the lower panels of Fig. 2.

Figures 2 also shows the effect of the fundamental scale on visible energy and missing and visible transverse momentum. Increasing  $M_\star$  leads to more massive BHs, i.e., higher multiplicity and harder quanta in the Hawking phase. Therefore, higher values of  $M_\star$  tend to produce larger  $\cancel{P}_T$ . The visible transverse momenta show a similar pattern. Observation of events with high  $\cancel{P}_T$  would indicate high values of  $M_\star$ , independently of the details of BH formation and the number of extra dimensions. If BHs are observed at the LHC, it is thus conceivable that  $M_\star$  could be measured to a certain degree of precision.

Changing the number of extra dimensions affects the BH mass and the missing and visible energy outputs. Graviton emission increases with the number of extra dimensions [33], leading to a decrease in visible energy for high  $n$ . The variation in  $\cancel{P}_T$  due change in spacetime dimensionality is

much less significant due to the high degree of sphericity of BH events (upper-right panels). Effects due to the dimensionality of spacetime are more evident for massive BHs, whereas most of the BHs produced at the LHC are very light. Therefore, it is likely that LHC would not be able to determine the number of extra dimensions just by statistical means.

Figure 3 shows the effects of varying the minimum mass lower bound. The distributions separate quite easily the two values of  $M_{min}$ . However, since  $M_{min}$  is a lower bound on the BH mass, increases in  $M_{min}$  are akin to increases in  $M_\star$  (compare the upper-left panels of Fig. 2 and Fig. 3). Changes in  $M_{min}$  are also entangled with the initial graviton emission, in particular for massive events: In the BD model, larger values of  $M_{min}$  (at fixed  $M_\star$ ) lead to more massive BHs, and thus to higher visible transverse momenta. If the initial gravitational emission is turned on, this increase may be balanced by a decrease due to lower multiplicity (compare  $M_{min} = 1$  TeV for the BD model with  $M_{min} = 2$  TeV for the YR model). A measure of  $M_{min}$  on purely statistical basis might prove to be difficult at the LHC.

Figure 4 displays the effects of the final BH decay (YR TS model). The distributions show that it is virtually impossible to distinguish the  $n_p = 2$  model from the  $n_p = 4$  model. Although quanta emissivities in the Hawking phase and the final phase differ for the presence of greybody factors in the former, the difference is not sufficient to allow a separation without a spectral analysis of the energy and the number of emitted quanta. The detection of a BH remnant stands a better chance because of larger  $\cancel{P}_T$  and smaller visible momentum due to its undetectability. (See also Refs. [42, 43].) Note that a large fraction of events with remnant produces very little visible output. This is due to the fact that most of the BHs are initially so light that the Hawking phase does not take place. For higher mass events, the energy carried by the decay products is much larger than the invisible energy carried by the remnant. Therefore, detection of a remnant is less likely in high-mass events.

Figure 5 compares a smooth spacetime and a spacetime with nonzero minimum length equal to the fundamental Planck scale inverse. The plots show no significant statistical differences between the two cases. The effects of a small distance cut-off becomes only relevant when the minimum scale is very close to the threshold of complete suppression of BH production, i.e., when the minimum allowed mass Eq. (2) is so large that BHs cannot form at the LHC CM energy. Therefore, observation of minimum length effects at the LHC requires a certain degree of fine tuning in the parameter  $\alpha$ .

## 4.2 Sphericity, thrust and Fox-Wolfram moments

BH events are expected to be highly spherical because of the spherical nature of Hawking evaporation. The event shape can be quantified by means of the sphericity  $S$  and aplanarity  $A$  [50], thrust and oblateness  $T$  [51], and Fox-Wolfram moment  $R_1 \dots R_4$  variables [52]. Fig. 6 shows sphericity, aplanarity, oblateness and thrust for

$$M_\star = 1 \text{ TeV}, \quad n = 6, \quad M_{min} = Q_{min} = M_\star, \quad \alpha = 0,$$

BD and TS models and different final decay modes ( $n_p = 2, 4$ ), respectively. (Rare) massive BH events are characterized by very high sphericity and isotropy. A similar conclusion is reached by examining the second Fox-Wolfram moment (see first panel of Fig. 7). Increasing  $M_{min}$  makes the events even more spherical because of the higher multiplicity in the decay phase.

Comparison between BD and TS models at fixed  $n_p$  shows that the BD model leads on average to more spherical events. This is expected because BD BHs are more massive and emit more quanta in

the Hawking phase than TS BHs. The higher sphericity of BD events is evident from the central part of the distributions, where Hawking emission dominates the emission in the final explosive phase, making the statistical difference between BD and TS models more clear. Comparison between  $n_p = 2$  and  $n_p = 4$  at fixed BD or TS shows the former to be less spherical than the latter. This effect is better displayed in the region of the plots corresponding to light BHs, where emission in the final phase dominates over Hawking emission. However, it should be stressed that the distinction between  $n_p = 2$  and  $n_p = 4$  at the LHC might well prove impossible due to the presence of non-BH background. Distinction between BD and alternative models of BH formation should be possible by selecting massive spectacular events with high sphericity.

### 4.3 Heavy and light jet mass

The upper-right and the lower panels of Fig. 7 show the number of jets and heavy and light jet mass [11] for the choice of parameters discussed above, respectively. Note that these plots include initial- and final-state radiation jets in addition to the jets originated by the BH decay phase. The BD model produces on average more jets than the TS model (upper-right panel of Fig. 7). This is also evident from the right portions of the jet mass distributions, where the BD model is characterized by more massive jets than the TS model at fixed  $n_p$ . Therefore, measurement of high jet mass allows determination of the BH formation model independently of the shape variables. The left portions of the jet mass distributions are sensitive to the final BH decay. Final decay in two jets produces more heavy jets than final decay in four jets at fixed BD or TS model. Therefore, the measurement of low jet mass may give important information on the physics of the final BH phase.

## 5 Conclusions and further developments

The study of BH production at the TeV scale is now a few years old and entering the mature stage. Although some of the characteristics of subatomic BH production remain obscure, many new theoretical results have been published in the literature. A MC generator which includes these theoretical results is needed for accurate simulations of BH events at the forthcoming LHC. Such a generator is also important to check the stability of the overall picture of BH production against improvements in the theory and have independent confirmation of previous results obtained with existing generators. With this in mind, we have developed CATFISH. The CATFISH generator implements several features of BH production at the TeV scale which were not included in TRUENOIR and CHARYBDIS. CATFISH new physics includes inelasticity effects during the BH formation phase [17, 18], exact field emissivities (albeit only for non-rotating BHs) [33], corrections to Hawking's semiclassical evaporation phase [29, 30], BH recoil on the brane, and different final BH decay modes with possibility of remnant formation [42]. These features allow the most accurate description of BH events at the TeV scale up-to-date. Another important feature of CATFISH is its flexibility. CATFISH design based on independent subroutine blocks allows easy inclusion of new theoretical results as soon as they become available. For example, the most significant changes to the phenomenology of BH formation in particle colliders is expected to arise from spin and charge effects. Emissivities for rotating and/or charged BHs can be easily implemented in CATFISH if known. We are also planning to include in future versions of the MC generator backreaction effects during the Hawking phase (see, e.g., Ref. [45]), thermodynamic fluctuations [30], SUSY effects [35] and photosphere and chromosphere effects [53].

The analysis of BH formation presented in the second part of this paper is limited to a few

statistical observables. This represents by no means CATFISH full potentiality. Several other interesting signatures of BH formation in particle colliders have been investigated in the literature (see, e.g., Refs. [43, 44, 46, 47, 48]). In particular, suppression of high-energy back-to-back-correlated di-jets with energy above the fundamental scale and di-lepton production with large transverse momentum are expected to be two of the most interesting signatures of BH production at the LHC. Investigation of these signatures with CATFISH is in progress [49]. Finally, detector response and event reconstruction are also fundamental issues to be addressed in a complete analysis of BH events at the LHC. Further work along these lines is currently being pursued. Precompiled executable Linux and Mac OS versions of CATFISH can be downloaded at the CATFISH website: <http://www.phy.olemiss.edu/GR/catfish>.

## Acknowledgments

The authors would like to thank Vitor Cardoso, David Cline, Greg Landsberg, Alexander Melnitchouk, Robert Palmer, David Sinn, Janes Pinfeld, Hans Wenzel and Graham Wilson for discussions and many useful suggestions. This work was supported in part by the U.S. Department of Energy contract DE-FG05-91ER40622.

## References

- [1] N. Arkani-Hamed, S. Dimopoulos and G. R. Dvali, *Phys. Lett. B* **429** (1998) 263;  
I. Antoniadis *et al.*, *Phys. Lett. B* **436** (1998) 257;  
N. Arkani-Hamed, S. Dimopoulos and G. R. Dvali, *Phys. Rev. D* **59** (1999) 086004.
- [2] R. Maartens, *Living Rev. Rel.* **7** (2004) 7.
- [3] T. Banks and W. Fischler, “A model for high energy scattering in quantum gravity,” arXiv:hep-th/9906038;  
S. B. Giddings and S. Thomas, *Phys. Rev. D* **65** (2002) 056010;  
S. Dimopoulos and G. Landsberg, *Phys. Rev. Lett.* **87** (2001) 161602;  
K. m. Cheung, *Phys. Rev. Lett.* **88** (2002) 221602;  
A. Chamblin and G. C. Nayak, *Phys. Rev. D* **66** (2002) 091901.
- [4] E. J. Ahn, M. Cavaglià and A. V. Olinto, *Phys. Lett. B* **551** (2003) 1;  
E. J. Ahn and M. Cavaglià, *Gen. Rel. Grav.* **34** (2002) 2037;  
K. Cheung and C. H. Chou, *Phys. Rev. D* **66** (2002) 036008.
- [5] M. Cavaglià, *Int. J. Mod. Phys. A* **18** (2003) 1843;  
G. Landsberg, *J. Phys. G* **32** (2006) R337;  
R. Emparan, “Black hole production at a TeV,” arXiv:hep-ph/0302226;  
P. Kanti, *Int. J. Mod. Phys. A* **19** (2004) 4899;  
S. Hossenfelder, “What black holes can teach us,” arXiv:hep-ph/0412265.
- [6] V. Cardoso, E. Berti and M. Cavaglià, *Class. Quant. Grav.* **22** (2005) L61.
- [7] S. W. Hawking, *Commun. Math. Phys.* **43** (1975) 199 [Erratum-*ibid.* **46** (1976) 206].
- [8] D. Amati and J. G. Russo, *Phys. Lett. B* **454** (1999) 207.

- [9] S. Dimopoulos and G. Landsberg, in: *Proc. of the APS/DPF/DPB Summer Study on the Future of Particle Physics (Snowmass 2001)* ed. N. Graf, eConf **C010630** (2001) P321.
- [10] C. M. Harris, P. Richardson and B. R. Webber, *JHEP* **0308** (2003) 033.
- [11] T. Sjostrand, S. Mrenna and P. Skands, *JHEP* **0605** (2006) 026.
- [12] E. Boos *et al.*, “Generic user process interface for event generators,” arXiv:hep-ph/0109068.
- [13] E. J. Ahn and M. Cavaglià, *Phys. Rev. D* **73** (2006) 042002.
- [14] R. Godang *et al.*, *Int. J. Mod. Phys. A* **20** (2005) 3409.
- [15] K.S. Thorne, in: *Magic without magic: John Archibald Wheeler*, ed. J. Klauder (Freeman, San Francisco, 1972).
- [16] M. B. Voloshin, *Phys. Lett. B* **518** (2001) 137;  
M. B. Voloshin, *Phys. Lett. B* **524** (2002) 376 [Erratum-ibid. *B* **605** (2005) 426];  
T. G. Rizzo, *JHEP* **0202** (2002) 011;  
V. S. Rychkov, *Phys. Rev. D* **70** (2004) 044003;  
S. B. Giddings and V. S. Rychkov, *Phys. Rev. D* **70** (2004) 104026.
- [17] H. Yoshino and Y. Nambu, *Phys. Rev. D* **67** (2003) 024009.
- [18] H. Yoshino and V. S. Rychkov, *Phys. Rev. D* **71** (2005) 104028.
- [19] O. I. Vasilenko, “Trap surface formation in high-energy black holes collision,” arXiv:hep-th/0305067.
- [20] P. C. Aichelburg and R. U. Sexl, *Gen. Rel. Grav.* **2** (1971) 303.
- [21] E. Kohlprath and G. Veneziano, *JHEP* **0206** (2002) 057.
- [22] V. Cardoso, O. J. C. Dias and J. P. S. Lemos, *Phys. Rev. D* **67** (2003) 064026.
- [23] E. Berti, M. Cavaglià and L. Gualtieri, *Phys. Rev. D* **69** (2004) 124011.
- [24] R. Brock *et al.* [CTEQ Collaboration], *Rev. Mod. Phys.* **67** (1995) 157.
- [25] W.-M. Yao *et al.* [Particle Data Group], *J. Phys. G* **33** (2006) 1.
- [26] E. J. Ahn, M. Ave, M. Cavaglià and A. V. Olinto, *Phys. Rev. D* **68** (2003) 043004.
- [27] R. Emparan, M. Masip and R. Rattazzi, *Phys. Rev. D* **65** (2002) 064023.
- [28] H. Yoshino, T. Shiromizu and M. Shibata, *Phys. Rev. D* **72** (2005) 084020.
- [29] M. Cavaglià, S. Das and R. Maartens, *Class. Quant. Grav.* **20** (2003) L205.
- [30] M. Cavaglià and S. Das, *Class. Quant. Grav.* **21** (2004) 4511.
- [31] G. Duffy, C. Harris, P. Kanti and E. Winstanley, *JHEP* **0509** (2005) 049;  
M. Casals, P. Kanti and E. Winstanley, *JHEP* **0602** (2006) 051;  
D. Ida, K. y. Oda and S. C. Park, *Phys. Rev. D* **71** (2005) 124039;  
D. Ida, K. y. Oda and S. C. Park, *Phys. Rev. D* **73** (2006) 124022.

- [32] P. Kanti and J. March-Russell, Phys. Rev. D **66** (2002) 024023;  
D. Ida, K. y. Oda and S. C. Park, Phys. Rev. D **67** (2003) 064025 [Erratum-ibid. D **69** (2004) 049901];  
P. Kanti and J. March-Russell, Phys. Rev. D **67** (2003) 104019;  
C. M. Harris and P. Kanti, JHEP **0310** (2003) 014;  
C. M. Harris and P. Kanti, Phys. Lett. B **633** (2006) 106;  
E. Jung and D. K. Park, Nucl. Phys. B **731** (2005) 171;  
A. S. Cornell, W. Naylor and M. Sasaki, JHEP **0602** (2006) 012;  
D. K. Park, Phys. Lett. B **638** (2006) 246.
- [33] V. Cardoso, M. Cavaglià and L. Gualtieri, Phys. Rev. Lett. **96** (2006) 071301 [Erratum-ibid. **96** (2006) 219902];  
V. Cardoso, M. Cavaglià and L. Gualtieri, JHEP **0602** (2006) 021.
- [34] M. Cavaglià, Phys. Lett. B **569** (2003) 7.
- [35] A. Chamblin, F. Cooper and G. C. Nayak, Phys. Rev. D **70** (2004) 075018.
- [36] V. P. Frolov and D. Stojkovic, Phys. Rev. D **66** (2002) 084002.
- [37] L. J. Garay, Int. J. Mod. Phys. A **10** (1995) 145.
- [38] M. Acciarri *et al.* [L3 Collaboration], Phys. Lett. B **470** (1999) 268;  
G. Abbiendi *et al.* [OPAL Collaboration], Eur. Phys. J. C **18** (2000) 253;  
A. Heister *et al.* [ALEPH Collaboration], Eur. Phys. J. C **28** (2003) 1;  
P. Abreu *et al.* [DELPHI Collaboration], Phys. Lett. B **485** (2000) 45;  
V. M. Abazov *et al.* [D0 Collaboration], Phys. Rev. Lett. **90** (2003) 251802;  
D. Acosta [CDF Collaboration], Phys. Rev. Lett. **92** (2004) 121802.
- [39] V. D. Barger, T. Han, C. Kao and R. J. Zhang, Phys. Lett. B **461** (1999) 34;  
S. Hannestad and G. Raffelt, Phys. Rev. Lett. **87** (2001) 051301;  
S. Hannestad and G. G. Raffelt, Phys. Rev. Lett. **88** (2002) 071301;  
M. Fairbairn, Phys. Lett. B **508** (2001) 335;  
L. J. Hall and D. R. Smith, Phys. Rev. D **60** (1999) 085008.
- [40] L. Randall and R. Sundrum, Phys. Rev. Lett. **83** (1999) 4690;  
L. Randall and R. Sundrum, Phys. Rev. Lett. **83** (1999) 3370.
- [41] H. L. Lai *et al.* [CTEQ Collaboration], Eur. Phys. J. C **12** (2000) 375.
- [42] B. Koch, M. Bleicher and S. Hossenfelder, JHEP **0510** (2005) 053.
- [43] H. Stocker, “Stable TeV - black hole remnants at the LHC: Discovery through di-jet suppression, mono-jet emission and a supersonic boom in the quark-gluon plasma,” arXiv:hep-ph/0605062.
- [44] C. M. Harris *et al.*, JHEP **0505** (2005) 053;  
B. Webber, eConf **C0507252** (2005) T030.
- [45] G. L. Alberghi *et al.*, “Probing quantum gravity effects in black holes at LHC,” arXiv:hep-ph/0601243.

- [46] J. Tanaka, T. Yamamura, S. Asai and J. Kanzaki, *Eur. Phys. J. C* **41** (2005) 19.
- [47] L. Lonnblad, M. Sjodahl and T. Akesson, *JHEP* **0509** (2005) 019.
- [48] G. C. Nayak and J. Smith, *Phys. Rev. D* **74** (2006) 014007.
- [49] M. Cavaglià *et. al*, “Black holes vs. SUSY at the LHC,” in preparation.
- [50] J. D. Bjorken and S. J. Brodsky, *Phys. Rev. D* **1** (1970) 1416.
- [51] S. Brandt, C. Peyrou, R. Sosnowski and A. Wroblewski, *Phys. Lett.* **12** (1964) 57.
- [52] G. C. Fox and S. Wolfram, *Phys. Rev. Lett.* **41** (1978) 1581;  
G. C. Fox and S. Wolfram, *Nucl. Phys. B* **149** (1979) 413 [Erratum-*ibid.* B **157** (1979) 543].
- [53] L. Anchordoqui and H. Goldberg, *Phys. Rev. D* **67** (2003) 064010;  
A. Casanova and E. Spallucci, *Class. Quant. Grav.* **23** (2006) R45.

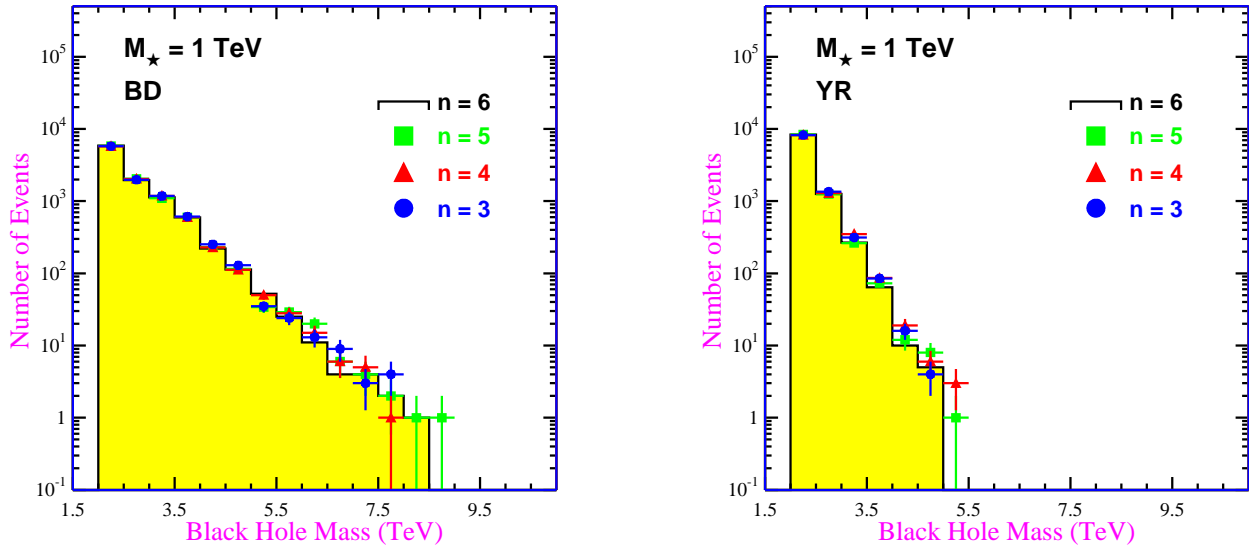


Figure 1:  $M_{BH}$  distribution for the black disk model (BD) and the Yoshino-Rychkov TS model (YR) and number of extra dimensions  $n = 3 \dots 6$ . The fundamental Planck scale  $M_*$  is 1 TeV.



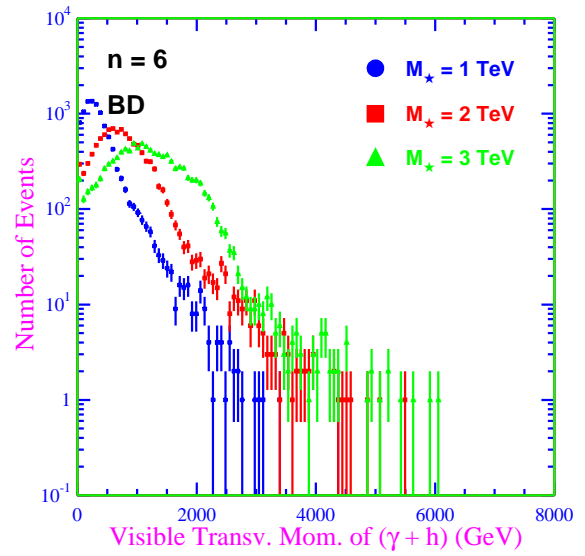
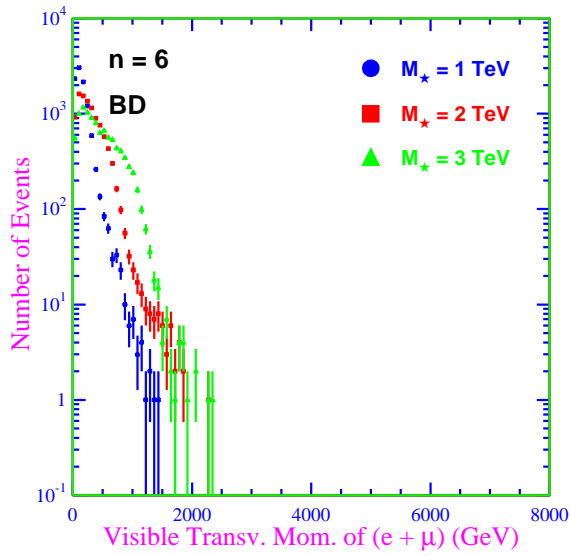
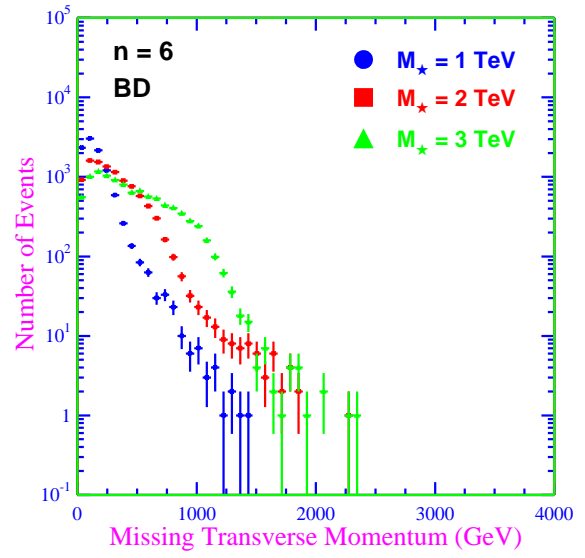
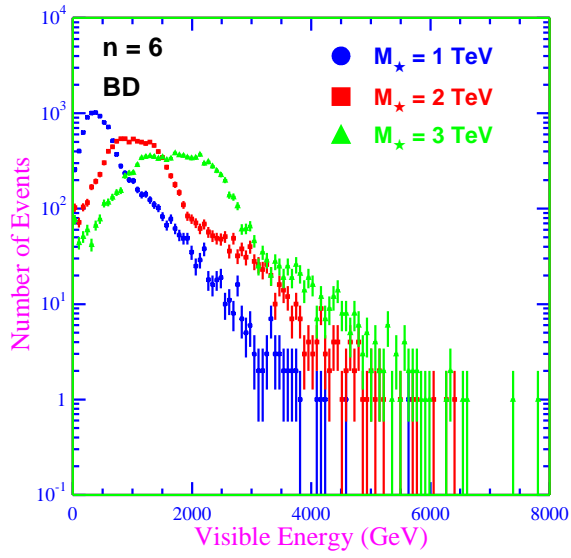


Figure 2: Visible energy,  $\cancel{P}_T$  and visible transverse momentum of leptons and photons+jets (GeV) for the black disk model (BD) and fundamental Planck scale  $M_* = 1, 2, 3$  TeV. The number of spacetime is ten-dimensional ( $n = 6$ ). The final BH decay is in  $n_p = 4$  quanta.

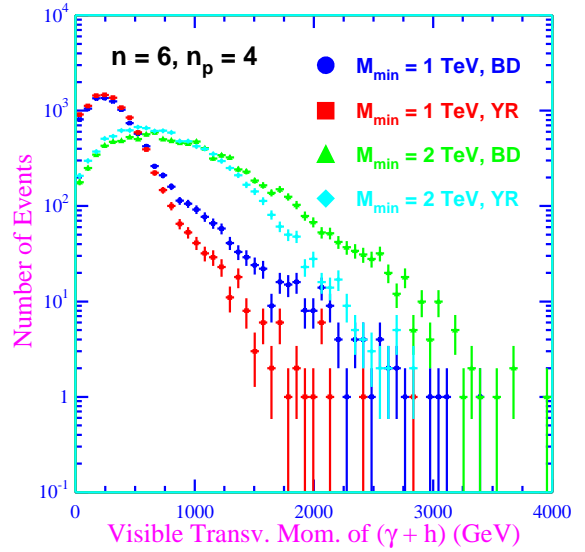
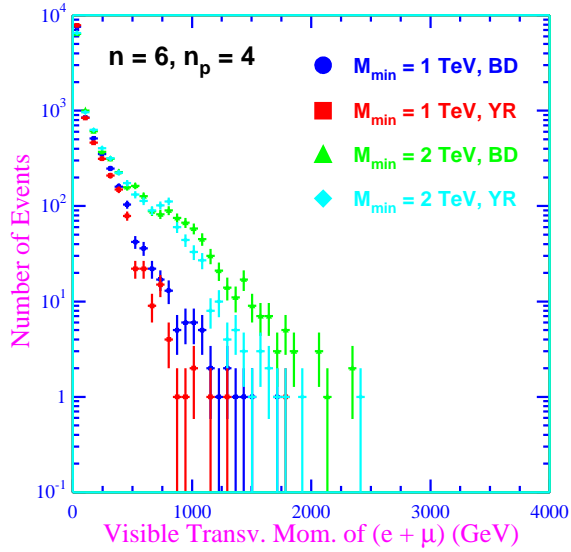
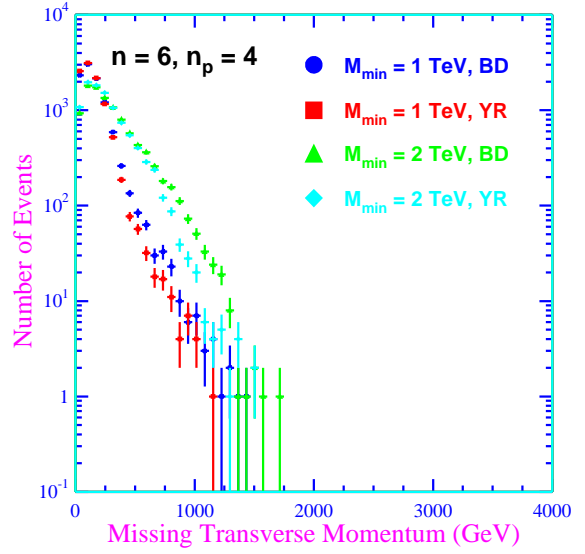
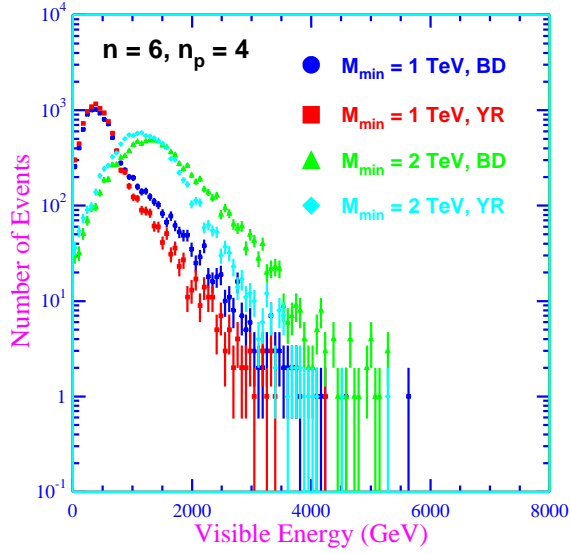


Figure 3: Visible energy,  $\cancel{P}_T$  and visible transverse momentum of leptons and photons+jets (GeV) for the black disk model (BD) and the Yoshino-Rychkov TS model (YR). The fundamental Planck scale is  $M_\star = 1$  TeV. The minimum formation mass of the BH is  $M_{min} = 1$  TeV or  $M_{min} = 2$  TeV. The final BH decay is in  $n_p = 4$  quanta.

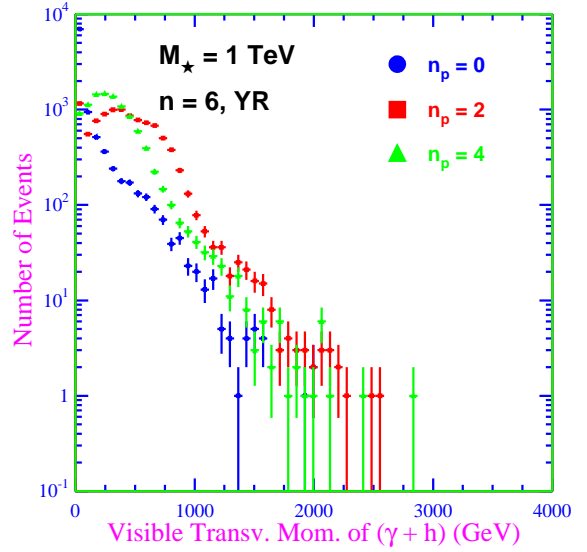
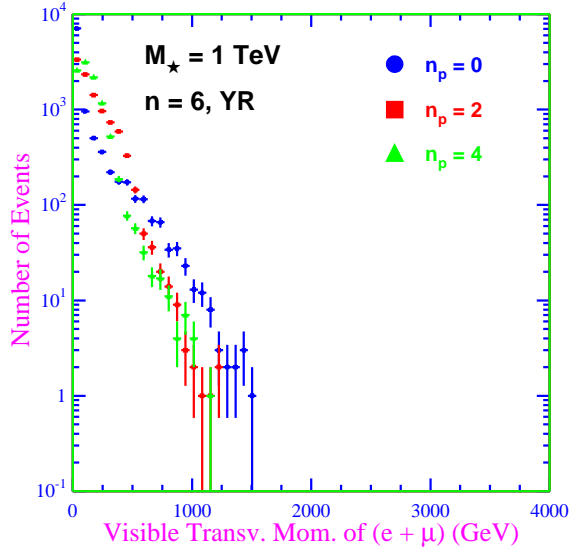
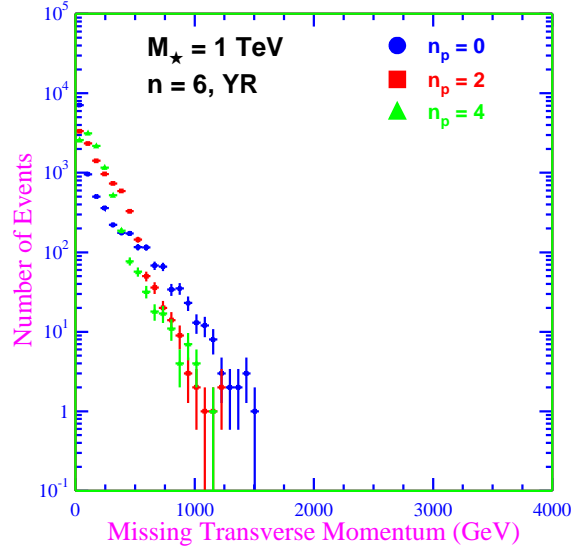
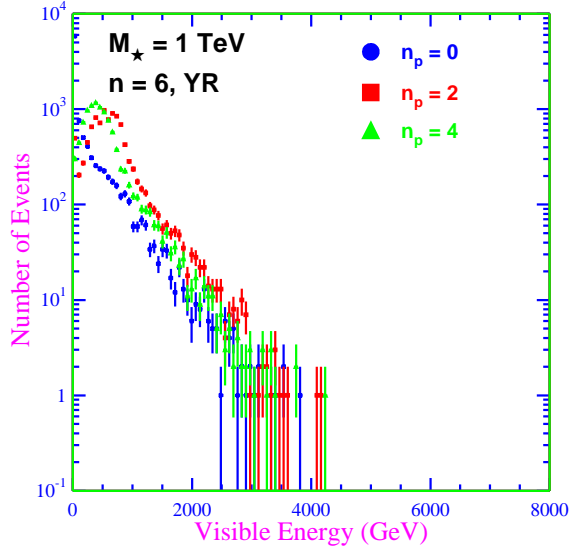


Figure 4: Visible energy,  $\cancel{p}_T$  and visible transverse momentum of leptons and photons+jets (GeV) for the Yoshino-Rychkov TS model (YR) with fundamental Planck scale  $M_\star = 1$  TeV and three different final decay modes: neutral remnant ( $n_p = 0$ ), two and four quanta.

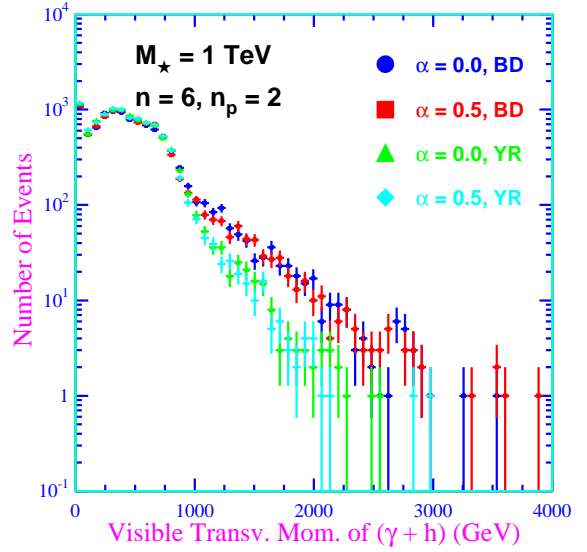
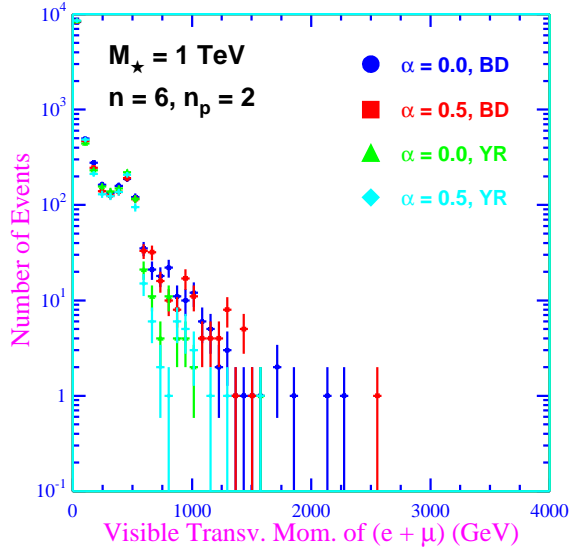
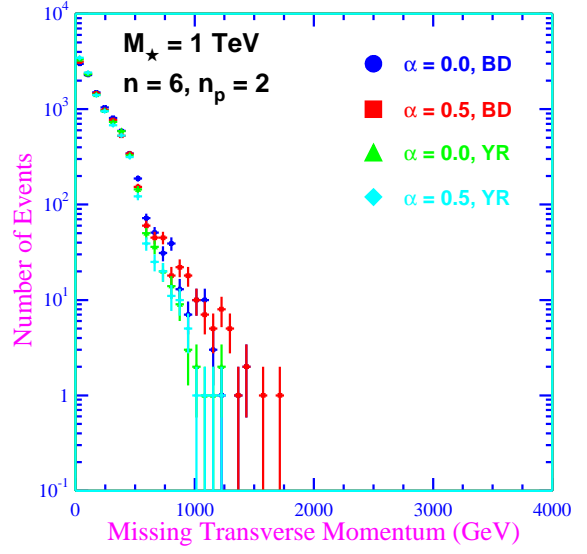
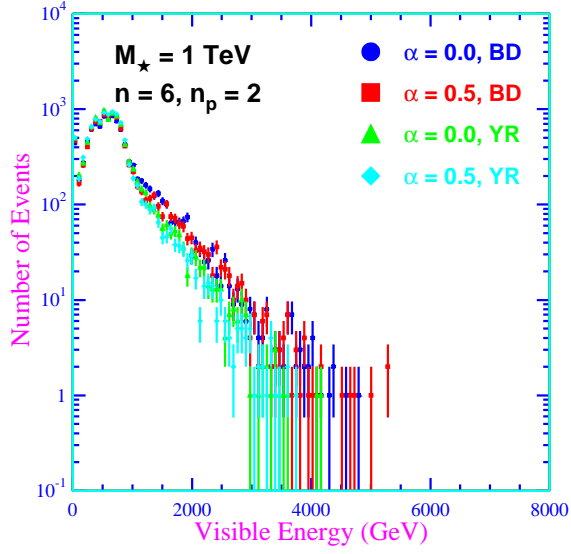


Figure 5: Visible energy,  $\cancel{P}_T$  and visible transverse momentum of leptons and photons+jets (GeV) for the black disk model (BD) and the Yoshino-Rychkov TS (YR) model with zero ( $\alpha = 0$ ) or  $M_*^{-1}$  ( $\alpha = 0.5$ ) minimum length. The final BH decay is in  $n_p = 2$  quanta.

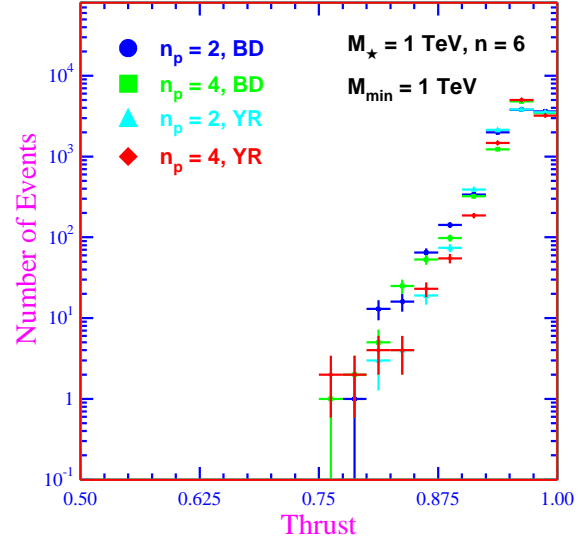
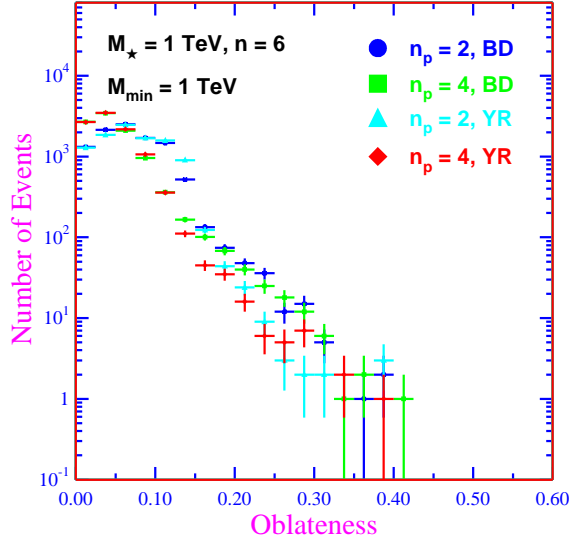
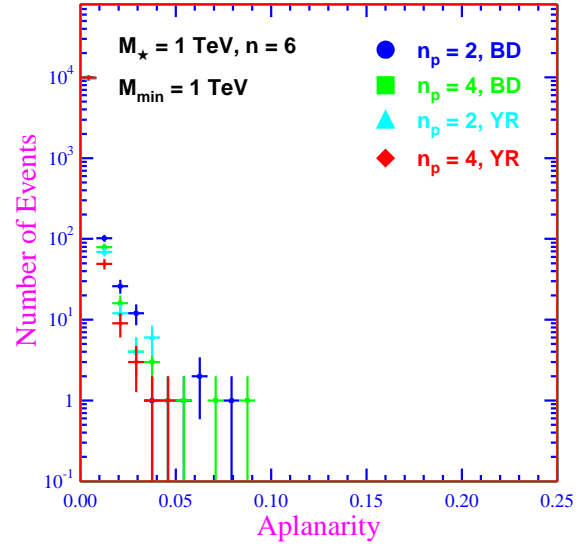
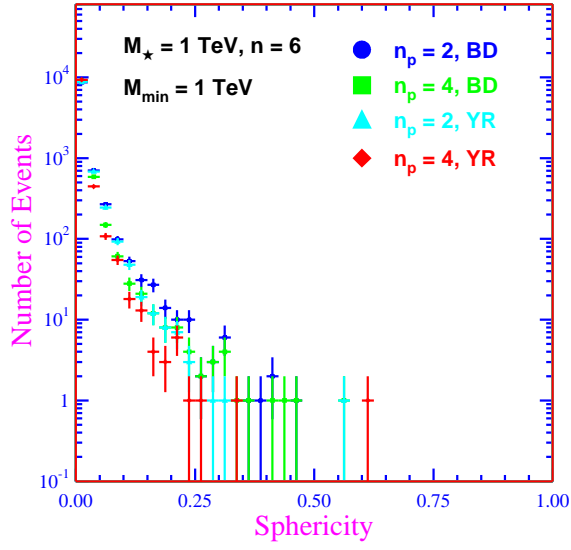


Figure 6: Sphericity, aplanarity, oblateness and thrust for the black disk model (BD) and the Yoshino-Rychkov TS model (YR). The final black hole decay is in two  $n_p = 2$  or  $n_p = 4$  quanta.

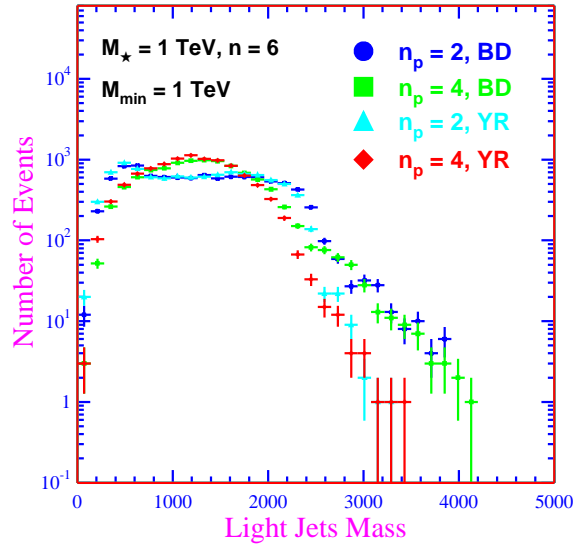
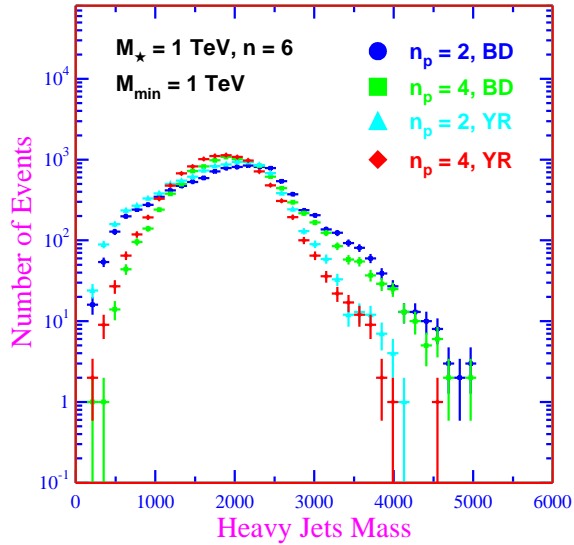
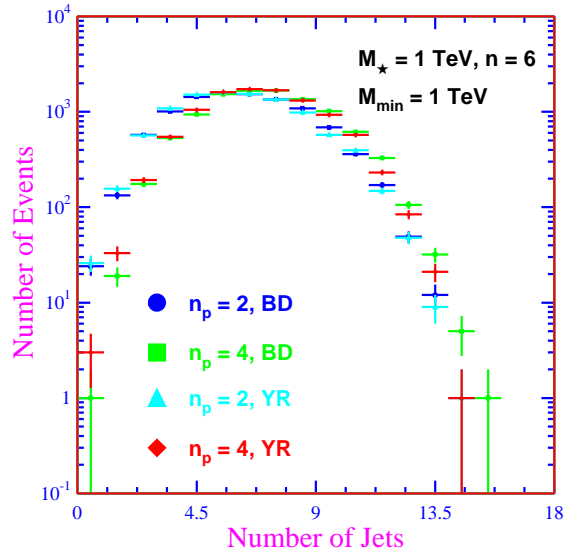
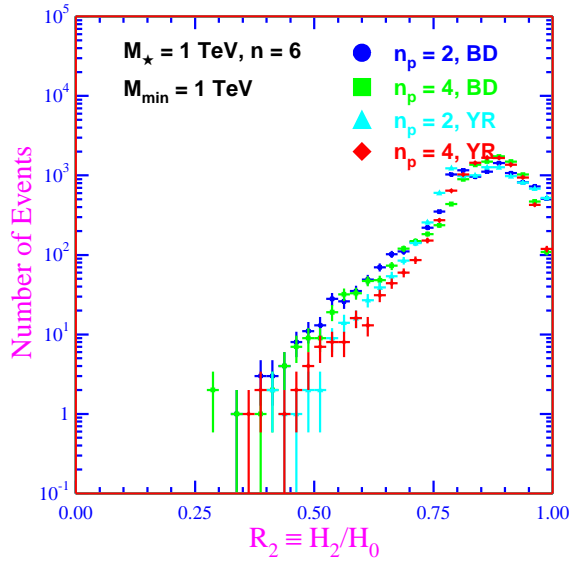


Figure 7: Fox-Wolfram moment  $R_2$ , number of jets, heavy and light jet mass for the black disk model (BD) and the Yoshino-Rychkov TS model (YR). The final black hole decay is in  $n_p = 2$  or  $n_p = 4$  quanta.